



Ground motion modelling in northwestern Himalaya using stochastic finite-fault method

Ramees R. Mir^{1,2} · Imtiaz A. Parvez^{1,2}

Received: 30 July 2019 / Accepted: 13 May 2020 / Published online: 31 May 2020
© Springer Nature B.V. 2020

Abstract

This study presents estimates of bedrock level peak ground motion at 2346 sites on a regular grid of $0.2^\circ \times 0.2^\circ$ in northwestern (NW) Himalaya from 543 simulated sources, using the stochastic finite-fault, dynamic corner frequency method, with particular emphasis on Kashmir Himalaya. The earthquake catalogue used for simulating synthetic seismograms is compiled by including both pre-instrumental and instrumental era earthquakes of magnitude $M_w \geq 5$, dating back to 260 AD. Acceleration time series thus generated are then integrated to obtain velocity and displacement time series, which are all used to construct a suite of hazard maps of the region. Expected PGA values for the Kashmir Himalaya and Muzaffarabad are found to be ~ 0.3 – 0.5 g and for the epicentral region of the 1905 Kangra event, to be 0.35 g. These values are consistent with other reported results for these areas e.g., Khattri et al. (Tectonophysics 108:93–134, 1984) and Parvez et al. (J Seismol, 2017. <https://doi.org/10.1007/s10950-017-9682-0>). The PGA values estimated in this study are in general found to be higher than those implied by the official seismic zoning map of India produced by the Bureau of Indian Standards (BIS in Indian Standard criteria for earthquake resistant design of structures part 1 general provisions and buildings (Fifth Revision), vol 1, no 5. Indian Standard, 2002). Even the acceleration-derived intensities for most regions are found to be higher compared with those observed, which apparently is due to the use of a longer duration catalogue (260 AD–2016) for simulation not covered by the observed intensity catalogue and higher magnitude ascribed to historical events. Major events in Kashmir Himalayas, such as those of 1555, 1885 and 2005, are simulated individually to allow comparison with available results. Simulated pseudo-acceleration and velocity response spectra for three sites near the 2005 Kashmir earthquake for which site conditions were available (Okawa in Strong earthquake motion recordings during the Pakistan, 2005/10/8, Earthquake, 2005. <https://iisee.kenken.go.jp>) are compared with observed spectra. This study provides a first-order ground motion database for safe design of buildings and other infrastructure in the NW Himalayan region.

Keywords Stochastic method · NW Himalaya · 2005 Kashmir earthquake · Seismic hazard

Both authors contributed equally to this work.

Electronic supplementary material The online version of this article (<https://doi.org/10.1007/s11069-020-04068-8>) contains supplementary material, which is available to authorized users.

Extended author information available on the last page of the article

1 Introduction

Over a dozen of damaging earthquakes have occurred along the Himalaya in the past millennium, including the 1555 (M_w 7.56) Kashmir, the 1905 (M_w 7.79) Kangra and the 2005 (M_w 7.6) Kashmir events, which took a huge toll of life and property. The NW Himalaya and adjacent regions, currently home to > 10 million people, also contain some prominent seismic gaps (Fig. 1) including the Kashmir Seismic Gap (KSG)—a seismically quiescent region since 1555 that lies between the rupture zones of the 2005 Kashmir and 1905 Kangra earthquakes (Khattri 1999). Meanwhile, a rapid increase in population, construction works and urban sprawls over the past half-century has resulted in exposing a much larger number of people and infrastructural assets to the repeated ineluctable seismic hazard of the region. The 1905 Kangra earthquake, which took a toll of 18,000 lives if it were to happen today, cause fatalities up to 80,000 even during daytime (Arya 1990). The number of people at risk in the region covering the

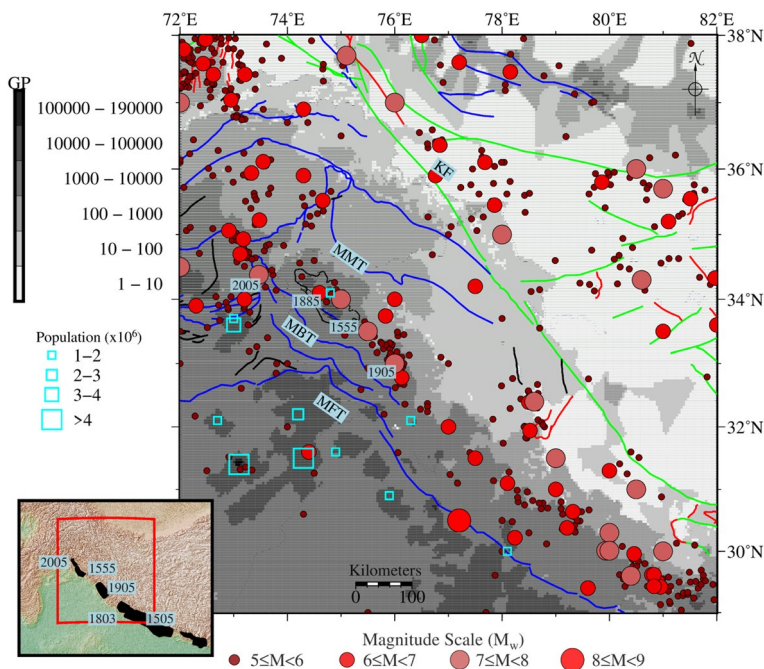


Fig. 1 Map of study region in NW Himalaya (29–38°N and 72–82°E). Earthquakes for period 260 AD to 2016, $M_w \geq 5.0$ (543 in number), are plotted and scaled in size according to their magnitude (see legend). Background shows adjusted gridded population (GP) ($5 \times 5 \text{ km}^2$) of the region (CIESEN 2018); note that the Himalaya and adjacent foreland basin is at substantial risk due to large population. Major thrust, normal, strike slip and unclassified faults are, respectively, shown by blue, red, green and black lines (Mohadjer et al. 2016). The main boundary thrust (MBT) and main frontal thrust (MFT) are major thrust systems of the NW Himalaya separating it into distinct litho-tectonic units but merge at depth into a decollement that marks the interface between the northward underthrusting Indian plate and Tibet that drives over it southwards. MMT is the Main Mantle Thrust and KF is Karakoram Fault. Population ($\geq 10^6$) of major cities are plotted as squares (see legend), with data obtained from the India census (2011), and Pakistan census (last accessed July 2017). Inset shows the location of study region (red rectangle) in the Himalaya along with major earthquake rupture zones marked by black polygons (Bilham 2019), clearly demarcating the current seismic gaps. Numbers represent the year of earthquake

present study can be gauged from the population in the region (Fig. 1), which has been steadily increasing. For example, in Srinagar, the capital city of the Kashmir valley, the population increased from 0.4 million in 1971 to 1.2 million in 2011 (Kuchay and Bhat 2014)—a threefold increase in just 40 years. The present work is motivated by the perceived need to produce knowledge-based figures of expected strong ground motion in the region to guide earthquake resistant design and construction practices.

Seismic hazard is defined as property of an earthquake which can cause damage or loss (McGuire 2004), and other associated effects can also be present like strong ground motion crossing a certain range, induced tsunami wave, landslides, rockfalls, liquefaction, etc. These can be evaluated using the Probabilistic Seismic Hazard Analysis (PSHA) or the Deterministic Seismic Hazard Analysis (DSHA) or a hybrid approach, depending on the data suite available. Seismic zoning map in India has been produced by the Bureau of Indian Standards (BIS) in terms of seismic zones numbered in ascending order of perceived seismic hazard intensity from 2 to 5. Additionally, several attempts were made to quantify seismic hazard using the meagre set of data available until recently. Notable amongst these are those by Khattri et al. (1984) and Bhatia et al. (1999). The first deterministic seismic hazard analysis of the Indian sub-continent was carried out by Parvez et al. (2003) followed by Kolathayar et al. (2012). Later, using updated input data and advanced computational tools, Parvez et al. (2017) produced a revised neo-deterministic seismic hazard map of India.

Here, we have simulated peak ground motions in terms of bedrock level acceleration, velocity and displacement at 2346 sites in northwestern Himalaya at $0.2^\circ \times 0.2^\circ$ spatial resolution, using the stochastic modelling approach introduced by Motazedian and Atkinson (2005) and subsequently modified by Boore (2009). This method simulates acceleration time histories using a combination of disaggregated finite-fault ruptures obeying the omega square model and a dynamic corner frequency. The method has been successfully used to simulate a number of scenario events, e.g. the 2011 (M_w 5.8) Mineral, Virginia (Sun et al. 2015); the 2015 (M_w 7.8) Gorkha, Nepal (Dhanya et al. 2017); and 2016 (M_L 6.6) Meinong, Taiwan (Chen et al. 2017) events.

The stochastic approach is well suited for evaluating peak ground motions in regions such as the NW Himalaya, where strong motion data are sparse. The approach allows efficient computation of ground acceleration time series at desired sites due to an earthquake of given seismic moment, by superposing individual accelerations produced by a set of discretized sub-faults that rupture sequentially. Simulated peak ground acceleration was also used to derive seismic intensities on the European Macroseismic Scale (EMS) following Panjamani et al. (2016) and Lliboutry (2000) and compared with observed intensities compiled by Martin and Szeliga (2010) (vide Online Resource Figure S1) also discretized at $0.2^\circ \times 0.2^\circ$ grid to allow point-to-point comparison. In particular, the simulated pseudo-acceleration and velocity response spectra (PAS, PVS) of the 2005 Kashmir earthquake have been compared with the observed response spectra available at three strong motion sites, using appropriate site amplification models guided by the available information (Okawa 2005).

2 Methods

Calculation of ground motion at a site (R) produced by a future damaging earthquake requires, at the very outset, knowledge of earthquake history of the region. In plate boundary regions such as the Himalaya, where accumulated strain energy from persistent tectonic activity is released periodically, the historical record should preferably cover at least one seismic cycle. In northwestern Himalaya where the annual convergence rate of ~ 12 mm adds $\sim 3 \times 10^{-19}$ Nm strain energy per year, a seismic cycle may be over a millennium or longer. The catalogue of events used for this work dates back to 260 AD, a period of over 1800 years, which we believe, fits this requirement. The basic quantity abstracted from the catalogue, apart from epicentral locations, is the homogenized value of seismic moment $M_0 = \mu A s$ where μ is the rigidity of the crust which has a value of $\sim 32 \times 10^9$ N/m². A is the total area of fault rupture and s is the total fault slip. In this work, we calculate ground accelerations, velocities and displacements at 2346 sites in northwestern Himalaya, first by defining the source parameters $S(M_0, \omega)$, of the strongest earthquakes that are known to have occurred in the region and propagating the released energy to calculate bedrock ground motion at various sites. Wherever these sites are overlain by unconsolidated materials with substantially different properties than those of hard rocks, we separately propagate the bedrock ground motion to the surface using knowledge of the overlying section. This is called correction for the site effect. In this study, we have used site effect only for 2005 M_w 7.6 Kashmir event to validate simulated pseudo-acceleration and velocity spectra with observed ones. Finally, the computed ground acceleration is integrated once to yield the surface velocity and twice to produce the ground displacement. Approximating the earth as a linear system, we can connect the above processes in terms of convolution (or multiplication in frequency (ω) domain) of source $[E(M_0, \omega)]$, path $[P(R, \omega)]$, and site $[G(\omega)]$ properties, i.e. $Y(M_0, R, \omega) = E(M_0, \omega)P(R, \omega)G(\omega)$. (See Sect. 2.2 for detailed description of this equation).

In this study, ground motions are generated using the finite-fault stochastic modelling method of Motazedian and Atkinson (2005). Accordingly, each fault surface is divided into a number of equi-dimensional sub-faults, each sub-fault being treated as a point source. The sizes of sub-faults are selected by optimizing the computational time: 1 km for $M_w < 6$, 3 km for $7 > M_w \geq 6$ and 6 km for $M_w \geq 7$. Slips on sub-faults are prescribed randomly subject to the total slip consistent with the seismic moment (M_0) of the particular earthquake. For each sub-fault, three random values of slip are chosen and average of these provides total slip from that sub-fault with rupture beginning from sub-fault near to the hypocentre. The major positive advantage accruing from the adoption of non-uniform slip is better representation at higher frequencies (Aki 1987). However, weakening of the directivity effect, i.e. less variation of amplitude w.r.t azimuth, above corner frequency of sub-faults is mostly caused by the use of large number of sub-faults (Galovič and Burjanek 2007).

Accelerations contributed by the various sub-faults (a_{ij}) that tessellate to form the entire rupture plane are then superposed to obtain the total acceleration produced by a given fault rupture.

$$a(t) = \sum_{i=1}^{nl} \sum_{j=1}^{nw} a_{ij}(t + \Delta t_{ij})$$

where nl and nw are, respectively, the index numbers of the sub-faults along the length and width of the rupture, which slip with time delays of Δt_{ij} .

2.1 From the Earthquake catalogue to the definition of its rupture parameters

The earthquake catalogue compiled here (260 AD to 2016) is assembled from various national and international agencies, notably the National Oceanic and Atmospheric Administration (NOAA), International Seismological Centre (ISC), United States Geological Survey (USGS), Indian Meteorological Department (IMD), National Disaster Management Authority (NDMA) and Global Earthquake Model (GEM) along with early instrumental and historical events compiled by various authors, notably Chandra (1978), Ambraseys and Douglas (2004) and Kolathayar et al. (2012) (for events $M_w \geq 7$). Also, the variously scaled magnitudes used by different authors have been translated into Moment magnitudes (M_w) following Scordilis (2006). This list is further scrutinized for any repetitions in time and space following Wiemer (2001). Also, all events lying within a square grid of $0.1^\circ \times 0.1^\circ$ are replaced by a single largest event. A total of 543 events (Fig. 1) thus screened have been used in quantifying seismic hazard in the region. The final compiled catalogue is available via Online Resource Table S1. Next, we parameterize each event in terms of their magnitude (M_w), stress drop, strike, dip, depth, fault type, fault length and width (Wells and Coppersmith 1994) and epicentral coordinates, whilst using a constant value of stress drop equal to 100 bars.

In order to specify the geometry of rupture, we compile ~ 300 focal mechanism solutions ($M_w \geq 5$) of events that occurred in the study region during 1977–2014, from the ISC source mechanism catalogue, as those reported by the global Centroid Moment Tensor catalogue are quite sparse during this very period. These events along with those from Khalid et al. (2016) are studied for their strike and dip variations, and we select an average dip of 40° , strike of 310° and a shear-wave velocity (V_s) of 3.7 km/s estimate from Mir (2020). As the major events in this region have largely thrust-type mechanism, occurring along the Main Himalayan Thrust, we assume that all ruptures are reverse thrusts. Simulations of all 543 events are also used to investigate the sensitivity of estimated PGA values to the assumed values of stress drop and dip by perturbing them through ± 20 bars and $\pm 10^\circ$ respectively (Online Resource Figures S2 and S3). To account for sensitivity of V_s on the estimated PGA, we perturbed its selected value by ± 0.1 km/s for M_w 7.6 October 2005 Kashmir event (Online Resource Figure S4).

2.2 Parameters used for computation

2.2.1 Source

The earthquake source $E(M_0, \omega)$ in this simulation is defined in terms of displacement on the fault, equivalent to the seismic moment M_0 abstracted from the catalogue, and a source time function proposed by Aki (1967). Aki (1967) proposed a model of slip in terms of its frequency spectrum, called the omega square model. Aki (1967) obtained this model by trial and error to fit the observed results of Berckhemer (1962), assuming self-similarity of the rupture process, distills out the value of $E(M_0, \omega) = CS_0 [1 + (\omega/\omega_0)^2]^{-1}$, where ω_0 is the ‘corner’ frequency that marks an inflexion in the observed spectra, and $S_0 = M_0 \omega_0^3 = \text{constant}$. The constant C is defined by as $C = R_{\theta\varphi} FV/4\pi\rho\beta^3 R_0$ (Boore 2003), where $R_{\theta\varphi}$ denotes the radiation pattern whose average is taken over an appropriate range of azimuths (θ) and take-off angles (φ); ρ is the density, β is the shear-wave velocity near the source, and R_0 a reference distance, usually set equal to 1 km. F represents the free surface amplification

(taken as 2, Boore 2003), and V represents the partitioning of shear-wave energy into its horizontal components. Hypocentral depth of all events is assigned as a function of magnitude following Parvez et al. (2003) (Table 1).

Motazedian and Atkinson (2005) proposed the use of a dynamic corner frequency calculated in each simulation from the distribution of slips on the sub-faults. For a sub-fault rupturing at time t , a new corner frequency is calculated by considering the number of sub-faults ruptured till t and their average seismic moment. Therefore, ω_0 has a maximum value as rupture begins and decreases as rupture propagates. The use of a dynamic corner frequency that is shown to make ground motion estimates independent of the sub-fault size and number (Motazedian and Atkinson 2005) thus becomes the key advantage offered by stochastic methods.

2.2.2 The propagation term $P[R_s, Q, \omega, \beta]$

This term can be fundamentally derived from the elastodynamic Green’s Function (Aki and Richards 2002) but turns out to be quite unwieldy for calculating ground motion caused by a double-couple rupture. Fortunately, however, this term can be approximated by a general function of form $Z(R)\exp(-\omega R/2Q\beta_Q)$ where Q is seismic attenuation determined using velocity β_Q and $Z(R)$ —geometrical spreading—is represented by piecewise linear function defined as follows after Boore (2003) [Eq. 9]:

$$Z(R) = \begin{cases} \left(\frac{R_0}{R}\right), & R \leq R_1 \\ Z(R_1)(R_1/R)^{p_1}, & R_1 \leq R \leq R_2 \\ \dots & \\ \dots & \\ Z(R_n)(R_n/R)^{p_n}, & R_1 \leq R \leq R_2 \end{cases}$$

Here, we use three piecewise straight linear functions (Parvez et al. 2001) as follows: $R_0 = 1$ km; $p_1 = -0.9$, $R_1 = 1$ km; $p_2 = +0.2$, $R_2 = 70$ km and $p_3 = +0.7$, $R_3 = 500$ km. We also use path duration model of Boore and Thompson (2014) (Table 2), developed for active continental regions.

2.2.3 The site effect $G(\omega)$

Site conditions, if different from bedrock, allow a wide variety of influences in modifying the local ground motion. In general, they consist of two factors, one causing amplification and the other diminution. Following Boore (2003), we express this as— $G(\omega) = A(\omega)D(\omega)$ where $A(\omega)$ denotes amplification and $D(\omega)$ —the diminution. $A(\omega)$ is the effect produced by the vibration of the overburden column which has a node at the bottom and an anti-node

Table 1 Hypocentral depth (km) as a function of magnitude (M_w) used in all computations (after Parvez et al. 2003)

Magnitude (M_w)	Assigned depth (km)
$M_w \leq 7$	10
$8 > M_w > 7$	15
$M_w \geq 8$	25

Table 2 Parameters used for all simulations

Factor	Parameter	Representative value	Reference (if any)
Source	Fault plane	Length (km); width (km) Strike 310; Dip $40 \pm 10^\circ$; Depth: as per Table 1	Wells and Coppersmith (1994), ISC catalogue ($M_w > 7$ events), Khalid et al. (2016)
	Slip distribution	Random slip; 3 models per sub-fault	
	Stress drop	100 bars, 80 bars	
	Moment magnitude	From catalogue	
	Shear-wave velocity (β)	3.7 ± 0.1 km/s	Mir (2020)
	Density (ρ)	2.8 g/cm ³	
	Pulsing percentage	50%	Motazedian and Atkinson (2005)
	Rupture propagation velocity	0.8β	
Path	Quality factor	$Q = \max(Q_{\min}, Q_0 f^\eta)$ $Q_{\min} = 60, Q_0 = 180, \eta = 0.45$	Parvez et al. (2003)
	Path duration	Path distance (PS in km) and path duration (PD in s), slope: 0.156 PS(km), PD(s); 0, 0; 7, 2.4; 45, 8.4; 125, 10.9; 175, 17.4; 270.0, 34.2	Boore and Thompson (2014)
Site	Geometric spreading	$R_0 = 1$ km; $p_1 = -0.9, R_1 = 1$ km; $p_2 = +0.2, R_2 = 70$ km and $p_3 = +0.7, R_3 = 500$ km	Section 2.2
	Crustal amplification	General crustal amplification for Active Continental Regions	Boore and Thompson (2014)
	Site amplification	Only for M_w 7.6 Kashmir 2005 event	Rodriguez-Marek et al. (2001), Okawa (2005)
	Kappa (κ)	0.04 with 5% damping	Mittal and Kumar (2015)

For details see Sect. 2.2

at the surface. $D(\omega)$, on the other hand, is caused by the loss of energy by viscous dissipation which can be expressed as: $D(\omega) = \exp(-\omega\kappa/2)$. Here we use a value of 0.04 for κ as proposed by Boore (2003) and optimized by Mittal and Kumar (2015) to fit their experimental data from western Himalaya.

Table 2 lists all the parameters of source, path and site used for simulation, which includes general crustal amplification model for active continental regions (after Boore and Thompson 2014) generated for velocity model for which $V_{s30} = 618$ m/s. It shall be noted that all computations to generate peak ground motion maps are performed on bedrock, which means no site effects are used in this study, except in case of 2005 M_w 7.6 Kashmir event (Table 2 and Sect. 3.3).

Figure 2 shows ground motion prediction equations (GMPE) for NW Himalaya from Parvez et al. (2001), along with those obtained from tuning the EXSIM algorithm (Motazedian and Atkinson 2005; M_w 5–8) using the parameters listed in Table 2 and discussed above. For comparison, we also plotted GMPE obtained by Joyner and Boore (1981) for Western United States and Ambraseys and Bommer (1991) for Europe. However, GMPE of Joyner and Boore (1981) deviate from those of Parvez et al. (2001) at larger distances (> 100 km), which will have an insignificant contribution towards the final product. This comparison of GMPE is necessary for seismic hazard assessment, as attenuation uncertainties contributes to most of the errors in final hazard maps, particularly in strong motion data deficit region like the Himalaya.

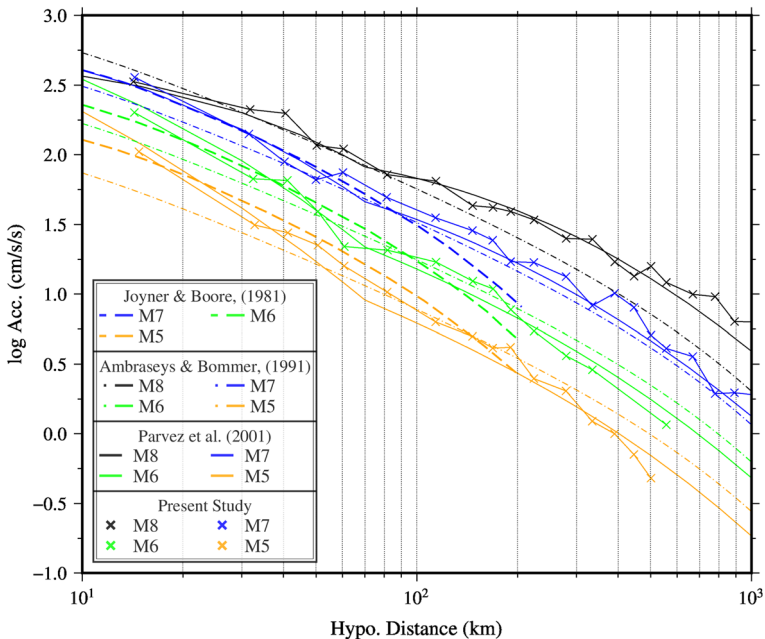


Fig. 2 Ground motion prediction equations (GMPE) obtained from tuning the EXSIM algorithm (Motazedian and Atkinson 2005; M_w 5–8) using the parameters listed in Table 2. For comparison GMPE for NW Himalaya (Parvez et al. 2001), Western United States (Joyner and Boore 1981) and Europe (Ambraseys and Bommer 1991) are also plotted (see legend)

3 Simulation results

Synthetic seismograms are simulated in northwestern Himalaya (29–38°N and 72–82°E) at each $0.2^\circ \times 0.2^\circ$ grid point using the EXSIM12 algorithm of Motazedian and Atkinson (2005). The process for identifying the peak acceleration time series from those generated by all the 543 events is automated for a group of 50 sites at a time, and the procedure is repeated for all other sites. The maximum of 543 acceleration time series thus computed for each of the 2346 sites is finally retained. These are shown in Fig. 3. Since we obtain acceleration time series using the EXSIM12 algorithm, the omega arithmetic method is used for integrating accelerations to velocity and displacement. In this method, acceleration time series are Fourier-transformed and divided with $j\omega$ to obtain the corresponding velocity and further converted back into time domain using an inverse Fourier transform (Brandt and Brincker 2014). A similar procedure is followed to obtain displacement time series along with a high-pass filter of corner frequency 0.1 Hz to attenuate the long-period effects. The generated peak ground motion maps of velocity and displacement are shown in Fig. 4.

PGA values for the Kashmir Himalaya are found to vary from 0.3 to 0.5 g. It is observed as: 0.33 g for the capital city of Srinagar, 0.39 g for Kupwara, near the north-western edge of the Kashmir basin (KB) and 0.47 g for Anantnag, near its south-eastern edge. PGA values north of the Main Frontal Thrust (MFT) are generally higher: 0.44 g

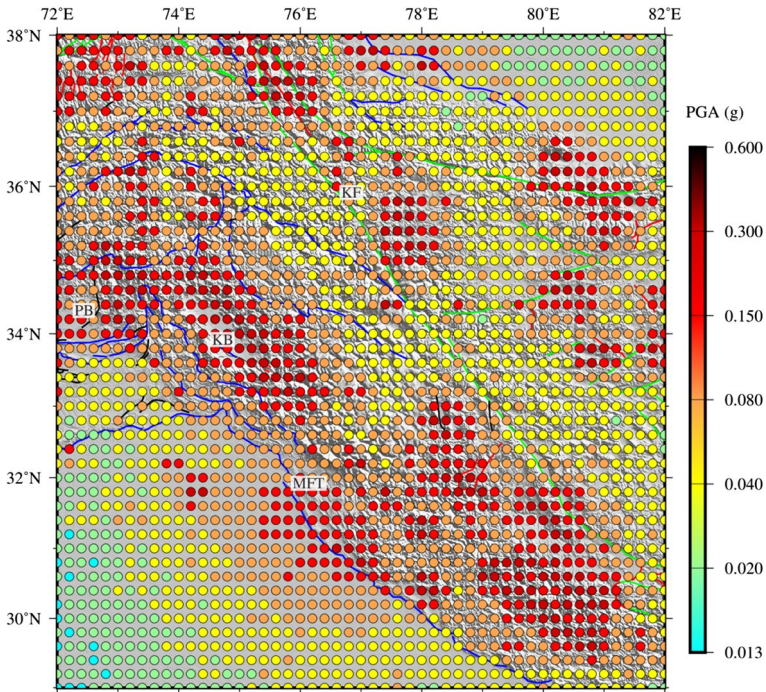


Fig. 3 Peak ground acceleration map (in g) at bedrock level at all 2346 sites; dip 40° , strike 310° and stress drop of 100 bars. All 543 earthquakes were simulated, acceleration time series are generated at each site and maximum PGA are picked to map. MFT is the Main Frontal Thrust, KF is Karakoram Fault, and KB and PB are Kashmir and Peshawar Basins in NW Himalaya. Faults are same as in Fig. 1

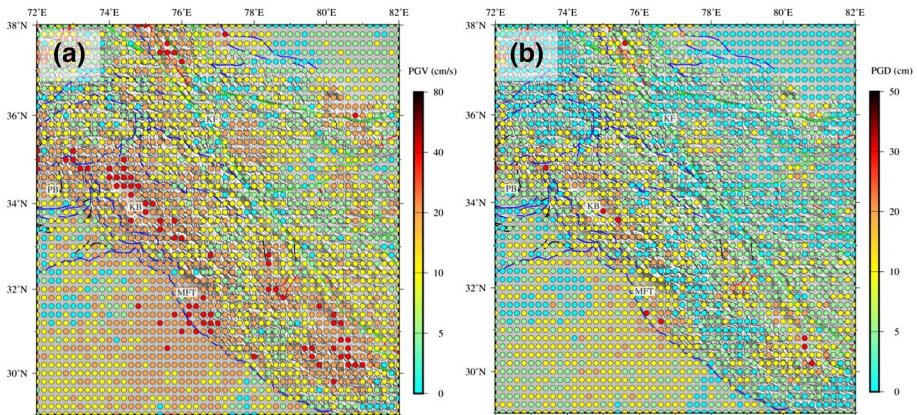


Fig. 4 **a** Peak ground velocity map (in cm/s) and **b** peak ground displacement map (in cm) at all sites with parameters same as in Fig. 3. The peak displacement values are picked after applying a high-pass filter of corner frequency 0.1 Hz to obtained displacement time series. Faults are same as in Fig. 1

near the south-eastern edge of the valley, 0.3 g in the Peshawar basin (PB) and 0.3–0.35 g in Himachal Himalaya including the epicentral region of the 1905 Kangra earthquake. A comparatively smaller value of 0.07–0.09 g is found for the Zaskar range NE of the Kashmir basin (Fig. 1), likely reflecting the lack of seismicity over the steady convergence slip zone that lies deeper below. In the Jammu region too, south of the MFT, PGA values are found to be much lower: 0.12 g. Table 3 compares the PGA values obtained from the current study with those calculated by Bhatia et al. (1999), Giardini et al. (1999) and Parvez et al. (2017), and BIS (2002), for major cities in the region.

3.1 Comparison with observed intensities

To validate the simulated values of PGA, we convert these into EMS earthquake intensity scale following Panjamani et al. (2016) for comparison with the observed EMS intensities provided by Martin and Szeliga (2010), also discretized at $0.2^\circ \times 0.2^\circ$ to have point-to-point check. The discretized intensities from Martin and Szeliga (2010) available at 397 points from 39 events over a period of 374 years represent maxima of the observed intensity at each point. The difference between derived values and the observed ones ($dI = I_{\text{sim}} - I_{\text{obs}}$) is mapped in Fig. 5a. Out of the 397 points, about 56% sites have intensity difference within ± 1 i.e. $-1 \leq dI \leq +1$, $\sim 43\%$ show higher simulated intensity value $dI > 1$; the remaining 1% show lower simulated intensities, $dI < -1$. It is clear that simulated intensities are larger than the observed ones, which may be due to the lesser number of events for shorter time periods reported by Martin and Szeliga (2010) and higher magnitude reported for historical events. To test the former assumption, we simulate the same period catalogue (374 years, 1636–2009) to generate peak ground acceleration map with same parameters as mentioned in Sect. 2. This new partial catalogue contains 35 lesser events, with 2 events having M6–6.9, 2 with $M > 7$ and rest lie in magnitude range of 5–5.9. The resulting acceleration and intensity difference maps are shown in Online Resource vide Figure S5, which show lesser difference between simulated and observed intensities as compared to full catalogue (Fig. 5a). With partial catalogue, about 70% sites now have intensity difference within ± 1 i.e. $-1 \leq dI \leq +1$, only $\sim 28\%$ show higher simulated intensity value $dI > 1$; the

Table 3 PGA from current and other studies for cities with population $\geq 10^6$ (Fig. 1)

City	Location (Lat°, Lon°)	PGA ^a (g) current study)	PGA(g)	Reference
Amritsar	31.6; 74.9	0.12	0.11	Parvez et al. (2017)
			0.12	BIS (zone) ^b
			0.15–0.20	Bhatia et al. (1999)
Dehradun	30.4; 78.0	0.33	0.30	Parvez et al. (2017)
			0.12	BIS (zone) ^b
			0.25–0.3	Bhatia et al. (1999)
Faisalabad	31.4; 73.1	0.08	0.20	Giardini et al. (1999)
Gujranwala	332.2; 74.2	0.07	0.23	Giardini et al. (1999)
Haridwar	30.0; 78.1	0.09	0.20	Parvez et al. (2017)
			0.12	BIS (zone) ^b
			0.15–0.2	Bhatia et al. (1999)
Islamabad	33.7; 73.0	0.10	0.26	Giardini et al. (1999)
Jalandar	31.3; 75.6	0.15	0.08	Parvez et al. (2017)
			0.12	BIS (zone) ^b
			0.05–0.10	Bhatia et al. (1999)
Jammu	32.7; 74.9	0.12	0.11	Parvez et al. (2017)
			0.12	BIS (zone) ^b
			0.05–0.10	Bhatia et al. (1999)
Kangra	32.1; 76.3	0.14	0.15	Parvez et al. (2017)
			0.18	BIS (zone) ^b
			0.25–0.3	Bhatia et al. (1999)
Lahore	31.5; 74.3	0.17	0.24	Giardini et al. (1999)
Ludhiana	30.9; 75.9	0.08	0.14	Parvez et al. (2017)
			0.12	BIS (zone) ^b
			0.00–0.05	Bhatia et al. (1999)
Mandi	31.7; 76.9	0.13	0.15	Parvez et al. (2017)
			0.18	BIS (zone) ^b
			0.2–0.25	Bhatia et al. (1999)
Rawalpindi	33.6; 73.0	0.07	0.26	Giardini et al. (1999)
Sargodha	32.1; 72.7	0.03	0.23	Giardini et al. (1999)
Shimla	31.1; 77.2	0.21	0.52	Parvez et al. (2017)
			0.18	BIS (zone) ^b
			0.25–0.3	Bhatia et al. (1999)
Srinagar	34.1; 74.8	0.39	0.54	Parvez et al. (2017)
			0.18	BIS (zone) ^b
			0.2–0.25	Bhatia et al. (1999)

The estimated PGA from this study, given in column 3, represents maxima at a given location calculated by comparing over all considered events

^aFrom current study

^bAfterMenon et al. (2010)

remaining 2% show lower simulated intensities, $dI < -1$. For Himalaya, the resulting maps clearly show large differences in acceleration and intensity near the epicentral regions of

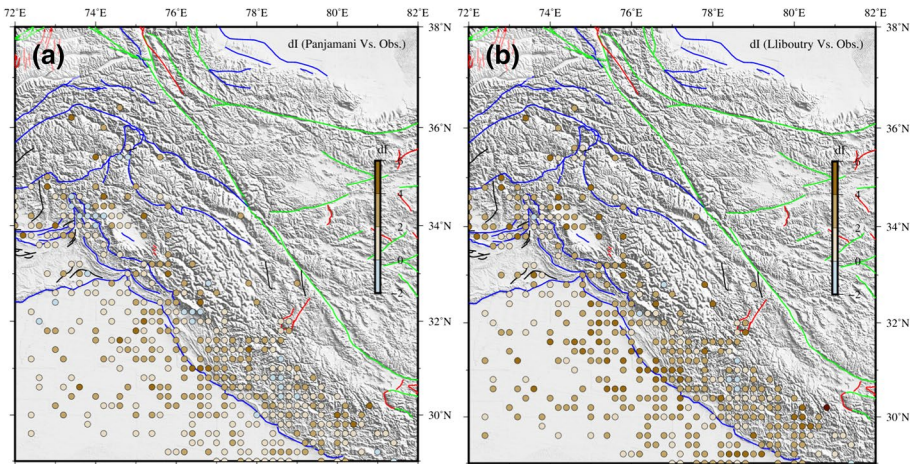


Fig. 5 **a** Difference between simulated and observed intensities ($dl = I_{sim} - I_{obs}$) with acceleration converted to intensity in EMS scale following Panjamani et al. (2016). **b** Same as in **a**, using Lliboutry (2000) for PGA to intensity conversions. Note that the estimated values are generally larger than observed ones, particularly while using conversion scheme of Lliboutry (2000). Faults plotted are same as in Fig. 1

260 AD M_w 8 Black Mango fault earthquake (Kumar et al. 2001) and 1555 Kashmir earthquake (M_w 7.56, Sect. 3.2), which are not covered in intensity catalogue of Martin and Szeliga (2010).

In fact, we repeat the above exercise by converting the simulated accelerations to EMS intensity using acceleration–intensity relationships of Lliboutry (2000). The resulting intensity difference map (Fig. 5b) is generated similarly by subtracting the observed values of Martin and Szeliga (2010) from the simulated ones. Figure 5b generally follows the dl trend of Fig. 5a, but with large differences. As acceleration to intensity relations of Panjamani et al. (2016) have been developed for the Himalayan region, apparently Fig. 5a is closer to observed intensities than Fig. 5b.

3.2 Historical events of 1555 and 1885

The September 1555 earthquake caused a significant loss of life in the Kashmir valley and its aftershocks reportedly rocked Kashmir and the adjoining areas for months. If we assume that the 1555 earthquake slipped by 5–6 m as required by the maximum estimated magnitude of M_w 7.56, the return time would be expected to be 500–600 years, given the observed geodetic convergence rate of ~12–14 mm/year. Thus, a recurrence of the 1555 earthquake would not be unexpected given the current state of knowledge. In order to have an estimate of its ground motion at bedrock, we simulate this event using the epicentral location (75.5°E, 33.5°N) given by Ambraseys and Douglas (2004), and the estimated PGA values are plotted in Fig. 6a. We also simulate the 1885 earthquake (Fig. 6b), which was one of the first events studied extensively (Jones 1885). It affected an area of about 1000 km², centred around NW edge of the Kashmir basin. Jones (1885) also reported a fissure of 1600 m in length and 7 m in width near Baramulla. We also study the directivity characteristics of this event through variations of waveforms with changing azimuth and fault

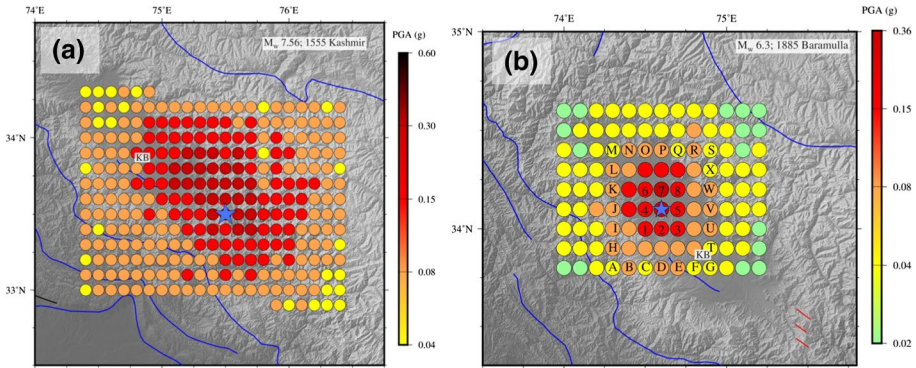


Fig. 6 **a** PGA map at $0.1^\circ \times 0.1^\circ$ for M_w 7.56, 1555 earthquake with same parameters as for Fig. 3. **b** Same as **a** for 1885 earthquake. Waveforms from labelled sites (1–8 and A–X) are plotted vide online resource Figure S6. Faults plotted are same as in Fig. 1

distance. Waveforms thus generated at some of the susceptible sites are plotted in Online Resource Figure S6, which demonstrates the absence of strong azimuthal dependence of simulated peak ground acceleration, despite the use of fixed value of strike (i.e. 310°).

3.3 The 2005 Kashmir event

The 2005 M_w 7.6 Kashmir earthquake is the only major event from the instrumental era to have been studied thoroughly. Accordingly, this event is also simulated here. This earthquake struck in the early hours of October 8, 2005 with its epicentre near Muzaffarabad. Its magnitude reported by Kaneda et al. (2008) was M_w 7.6 with a corresponding seismic moment of 2.9×10^{20} Nm, and it occurred at a depth of ~ 26 km. It had a strike direction of 333° and ruptured a series of faults collectively called the Balakot–Bagh fault system on a NE dipping fault with a dip of $\sim 40^\circ$. This event caused havoc and claimed about 80,000 lives; injured thousands and rendered many homeless. Fortunately, three strong motion records around the epicentre were available for comparison (Okawa 2005) proved especially valuable as they are recorded at sites with varying overburden conditions, which were also provided by Okawa (2005). Simulated PGA for this event is shown in Fig. 7, with rupture propagating towards the NW direction as suggested by teleseismic studies. The three sites at which strong motion recordings were available are Abottabad, Muree and Nilore (Fig. 7). Okawa (2005) provided acceleration and velocity response spectra for all three sites, which is compared with the spectra obtained here, after correcting for site effects according to the formulation of Rodriguez-Marek et al. (2001), by taking into account the site details provided by Okawa (2005) (Fig. 8). Rodriguez-Marek et al. (2001) introduced a site response evaluation method based on the stiffness of material and depth to bedrock level. Their classification scheme ranged sites from A–F, where A being hard rock and F potentially liquefiable sand. Since, as per Okawa (2005) Abbotabad site (Fig. 8a, b; ‘siteD-0.1 g’) is based on alluvium, we use site amplification of site D that represents stiff soil with site period < 1.4 s. Similarly, as per the details provided by Okawa (2005), Muree site (Fig. 8c, d) is apparently situated on a bedrock and hence no site amplification (Fig. 8c, d; ‘noamp’) is used to generate the spectra. Finally, for Nilore site a better fit between

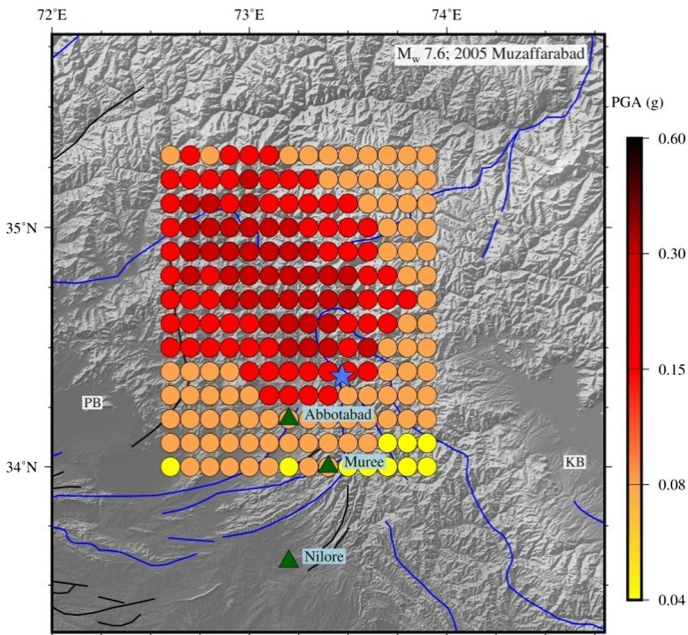


Fig. 7 PGA map for 2005 Kashmir earthquake (M_w 7.6) at bedrock level at $0.1^\circ \times 0.1^\circ$. Triangles represent three strong motion sites at which this event is recorded whose both acceleration and velocity response spectra were provided by Okawa (2005). This event has occurred near NW syntaxial bend of the Himalaya flanked on either side by basins of Kashmir and Peshawar (KB; PB). Faults plotted are same as in Fig. 1

observed and simulated spectra is obtained by not using both general crustal amplification (Boore and Thompson 2014; Table 2) as well as site amplification (Fig. 8e, f; ‘No-site-n-crustal-amp’), which could be due to high attenuation underneath.

4 Discussions and conclusion

Several authors have presented PGA maps of India at different times using data available to them and had employed different methodologies i.e. both PSHA and DSHA, with which the PGA obtained from this study is compared. Such comparisons are available in literature by considering PSHA maps generated using knowledge-based return period of large earthquakes in a given region (e.g. Zuccolo et al. 2011 for Italy). In the study region, a return period of 475 years (i.e. with 10% probability of exceedance in 50 years) is apparently realistic (e.g. see Sect. 3.2 for discussion on 1555 Kashmir earthquake). Hence, we refrain from comparing the obtained PGA values with studies of return period larger than 475 years. For example,

Rout et al. (2015) used both 2% and 10% probability of exceedance of PGA. Recurrence period of 2500 years (from 2% probability of exceedance) is unusable for describing earthquake probabilities in the Himalaya where return periods of M8 events are less than a 1000 years: 650 years for the Nepal Himalaya, (Sapkota et al. 2013), 350 years for 1905 Himachal event (Yeats and Thakur 1998), and similarly 530–720 years for Kashmir (Bendick et al. 2007).

Another set of PGA values from neo-deterministic method (Parvez et al. 2003, 2017), used for comparison here, is based on calculation of synthetic seismograms via modal summation technique of Panza et al. (2001). Comparison of PGA values obtained from this study and Parvez et al. (2003, 2017), while using region-specific parameters, e.g. attenuation and shear-wave velocity, provides a check of robustness for both the methodologies.

With these considerations, major studies using both PSHA and DSHA are briefly outlined below for comparison. Khattri et al. (1984) were the first to produce a probabilistic seismic hazard map of the country by considering linear sources. In the absence of data, Khattri et al. (1984) adopted GMPE at bedrock level from eastern US and used source depth of zero kilometres for all computations. Their maps show estimated PGA values with 10% probability of exceedance in 50 years (i.e. return period of 475 years). Khattri et al. (1984) estimated PGA for Kashmir Himalaya as ~0.4 g, close to 0.35 g value simulated in this study. Bhatia et al. (1999) also calculated PGA values for the India for 10% probability of exceedance in 50 years following Global Seismic Hazard Assessment Program (GSHAP) (Giardini et al. 1999). Their estimates of PGA for NW Himalaya are less than any of the earlier studies including the present one. Later, Mahajan et al. (2010), using the same GSHAP approach as Bhatia et al. (1999), produced an updated map with an augmented data set for probability exceedance of 10% over 50 years, their estimates for Kashmir Himalaya is about 0.35–0.7 g and that for Kangra region is 0.35–0.5 g. Rout et al. (2015) also used the PSHA methodology to determine PGA map for NW Himalaya at bedrock level with a grid size of $0.2^\circ \times 0.2^\circ$. They estimated PGA for 10% exceedance (return period of 475 years) as well as for 2% exceedance (return period of 2500 years). For 10% case, the maximum PGA in the study region is 0.36 g.

Parvez et al. (2003) produced the first deterministic earthquake hazard map of India by generating synthetic seismograms at 1 Hz at regular grid of $0.2^\circ \times 0.2^\circ$. For the western Himalaya, Parvez et al. (2003) estimated value of 0.3–0.6 g, which is similar to the value obtained in current study. Parvez et al. (2017) produced a revised neo-deterministic seismic hazard map. Table 3 shows a comparison of the PGA values in northwestern Himalaya determined by the various authors using varied data sets and methodologies. While comparing with the seismic zones provided by BIS (2002), the given zone values are converted to PGA using relations of Menon et al. (2010). The discrepancies noted here between deterministic and probabilistic approaches is expected, as argued by Parvez et al. (2003), because of the fundamental question asked by both, the former being, what could be the ground motion from a scenario event and latter being, what is the probability of exceeding value of a ground motion parameter in a particular time period.

We present in this study—PGA estimations in NW Himalaya using a stochastic approach that exploits the intrinsic relationships between fault rupture sources and self-similarity of the rupture processes to constrain the source model. PGA values thus calculated at 2346 sites with 0.2° resolution, covering an area close to a million square kilometres of northwestern Himalaya, provide a high resolution PGA map of the region. These calculations could be directly validated for just one event i.e., the 2005 Kashmir earthquake for which strong motion records generated at three different sites with varying overburden conditions were available. Close similarity of these observed spectra with those simulated for this earthquake using the stochastic approach lends confidence in the validity of this method that has been successfully tested elsewhere. However, we indirectly test PGA values simulated in this study by comparison of intensities derived from these values at each grid point with those observed and published. These successful comparisons engender confidence in the assertion that the PGA maps produced in this study provide a better estimate of earthquake hazard in the region.

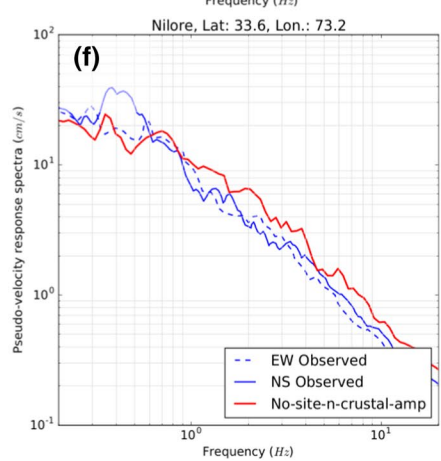
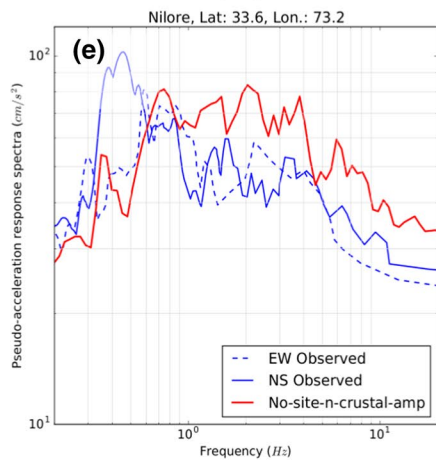
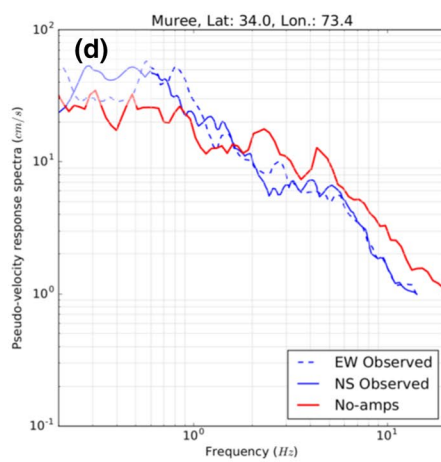
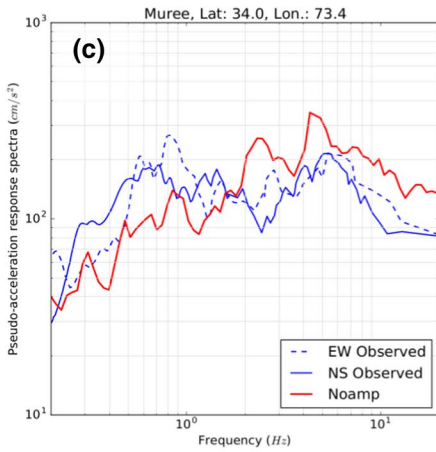
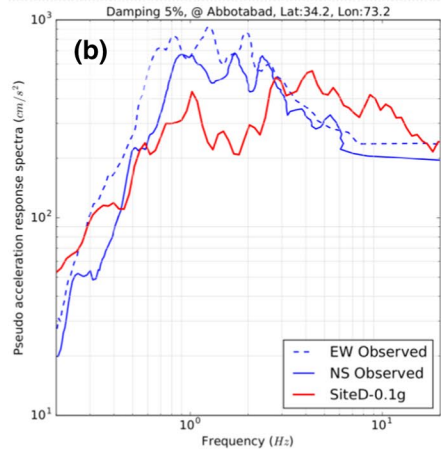
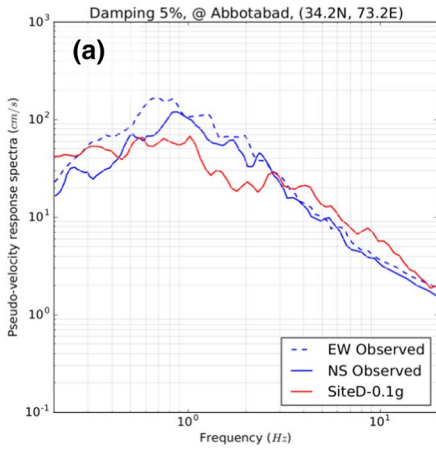


Fig. 8 Observed (blue) and simulated (red) pseudo-acceleration and velocity response spectra of Kashmir 2005 M_w 7.6 event for three sites Abbotabad (a, b), Muree (c, d) and Nilore (e, f) at damping of 5% and different site conditions. For Abbotabad site (a, b) the simulated spectra (red line) are obtained using site amplification of site D following Rodriguez-Marek et al. (2001) (see legend ‘siteD-0.1 g’). For Muree site (c, d) no site amplification is used (‘No-amps’), and for Nilore site (e, f) both general crustal amplification (Table 2) and site amplification are not used (‘No-site-n-crustal-amp’). For details see Sect. 3.3

Acknowledgements The authors would like to thank Prof. Vinod Gaur for his valuable comments and suggestions. We also acknowledge the continuous support provided by the Head, CSIR-4PI. We would also like to thank Dr. Stephan Crane for help on EXSIM12 algorithm. Sincere thanks to Prof. Thomas Glade and Prof. V. Schenk Editors-in-Chief at the *Natural Hazards* for their support. Comments from two anonymous reviewers helped a lot in improving this manuscript to its current shape. We acknowledge the financial support from Ministry of Earth Sciences (MoES), Government of India, via project number MoES/P.O.(Geosciences)16/2013 (GAP-1010). RM was also supported by Senior Research Fellowship from the Council of Scientific and Industrial Research (CSIR), New Delhi, India.

Compliance with ethical standards

Conflict of interest The authors declare that they have no conflict of interest.

References

- Aki K (1967) Scaling of the seismic spectrum. *J Geophys Res* 72(4):1217–1231
- Aki K (1987) Strong motion seismology. In: Erdik M, Toksz MN (eds) *Strong ground motion seismology*. Springer Netherlands, Dordrecht, pp 3–39. ISBN 978-94-017-3095-2
- Aki and Richards (2002) *Quantitative seismology*, 2nd edn. University Science Books, Mill Valley
- Ambraseys NN, Bommer JJ (1991) The attenuation of ground accelerations in Europe. *Earthq Eng Struct Dyn* 20:1179–1202. <https://doi.org/10.1002/eqe.4290201207>
- Ambraseys NN, Douglas J (2004) Magnitude calibration of north Indian earthquakes. *Geophys J Int* 159(1):165–206
- Arya AS (1990) Damage scenario of a hypothetical 8.0 magnitude earthquake in Kangra region of Himachal Pradesh. *Bull Indian Soc Earthq Technol* 27(3):121–132
- Bendick R, Bilham R, Khan MA, Khan SF (2007) Slip on an active wedge thrust from geodetic observations of the 8 October 2005 Kashmir earthquake. *Geology* 35(3):267–270. <https://doi.org/10.1130/G23158A.1>
- Berckhemer H (1962) Die ausdehnung der bruchflächeimerdbebenherd und ihreinflussauf das seismischewellenspektrum. *GerlandsBeitr Geophys* 71:5–26
- Bhatia SC, Kumar MR, Gupta HK (1999) A probabilistic seismic hazard map of India and adjoining regions. *Ann Geofis* 6:1153–1164
- Bilham R (2019) Himalayan earthquakes: a review of historical seismicity and early 21st century slip potential. In: Treloar PJ, Searle MP (eds) *Himalayan tectonics: a modern synthesis*. Geological Society of London, London. <https://doi.org/10.1144/SP483.16>
- BIS. IS 1893 (Part 1) (2002) Indian Standard criteria for earthquake resistant design of structures part 1 general provisions and buildings (Fifth Revision), vol 1, no 5. Indian Standard, New Delhi
- Boore DM (2003) Simulation of ground motion using the stochastic method. *Pure Appl Geophys* 160(3):635–676. <https://doi.org/10.1007/PL00012553>
- Boore DM (2009) Comparing stochastic point-source and finite-source ground-motion simulations: SMSIM and EXSIM. *Bull Seismol Soc Am* 99(6):3202–3216
- Boore DM, Thompson EM (2014) Path durations for use in the stochastic-methodsimulation of ground motions. *Bull Seismol Soc Am* 104(5):2541–2552
- Brandt A, Brincker R (2014) Integrating time signals in frequency domain—comparison with time domain integration. *Measurement* 58:511–519
- Chandra U (1978) Seismicity, earthquake mechanisms and tectonics along the Himalayan mountain range and vicinity. *Phys Earth Planet Inter* 16:109–131

- Chen C-T, Chang S-C, Wen K-L (2017) Stochastic ground motion simulation of the 2016 Meinong, Taiwan earthquake. *Earth Planets Space* 69(1):62
- CIESEN (2018) Center for International Earth Science Information Network, Columbia University. Gridded Population of the World, Version 4 (GPWv4): population count, revision 11. NASA Socioeconomic Data and Applications Center (SEDAC), Palisades. <https://doi.org/10.7927/H4JW8BX5>. Accessed 01 Mar 2020
- Dhanya J, Gade M, Raghukanth STG (2017) Ground motion estimation during 25th April 2015 Nepal earthquake. *Acta Geod Geophys* 52:69–93. <https://doi.org/10.1007/s40328-016-0170-8>
- Gallovič F, Burjanek J (2007) High-frequency directivity in strong ground motion modeling methods. *Ann Geophys* 50(2):203–211
- Giardini D, Gruenthal G, Shedlock K, Zhang P (1999) The global seismic hazard map. *Ann Geofis* 42(6):1225–1230.
- Jones EA (1885) Report on the Kashmir earthquake of 30th May 1885. *Rec Geol Soc India* 12(4):221–227
- Joyner WB, Boore DM (1981) Peak horizontal acceleration and velocity from strong motion records including records from the 1979 Imperial Valley, California, earthquake. *Bull Seism Soc Am* 71:2011–2038
- Kaneda H, Nakata T, Tsutsumi H, Kondo H et al (2008) Surface rupture of the 2005 Kashmir, Pakistan, earthquake and its active tectonic implications. *Bull Seismol Soc Am* 98(2):521–557
- Khalid P, Bajwa AA, Naem M, Di ZU (2016) Seismicity distribution and focal mechanism solution of major earthquakes of northern Pakistan. *Acta GeodGeophys* 51:347–357
- Khattri KN (1999) Probabilities of occurrence of great earthquakes in Himalaya. *Curr Sci* 77(7):967–972
- Khattri K, Rogers A, Perkins D, Algermissen S (1984) A seismic hazard map of India and adjacent areas. *Tectonophysics* 108:93–134
- Kolathayar S, Sitharam TG, Vipin KS (2012) Deterministic seismic hazard macro-zonation of India. *J Earth Syst Sci* 121(5):1351–1364
- Kuchay NA, Bhat MS (2014) Analysis and Simulation of urban expansion of Srinagar City. *Transt Inst Indian Geogr* 36(1):109–121
- Kumar S, Wesnousky SG, Rockwell TK, Ragona D et al (2001) Earthquake recurrence and rupture dynamics of Himalayan Frontal Thrust, India. *Sci Mag* 294:2328–2331
- Lliboutry L (2000) *Quantitative geophysics and geology*. Springer, London, 1st edn. ISBN 978-1-85233-115-3
- Mahajan AK, Thakur VC, Sharma ML, Chauhan M (2010) Probabilistic seismic hazard map of NW Himalaya and its adjoining area, India. *Nat Hazards* 53(3):443–457. <https://doi.org/10.1007/s11069-009-9439-3>
- Martin S, Szeliga W (2010) A catalog of felt intensity data for 570 earthquakes in India from 1636 to 2009. *Bull Seismol Soc Am* 100(2):562–569
- McGuire RK (2004) *Seismic hazard and risk analysis*. EERI. ISBN 0943198011
- Menon A, Ornthammarath T, Corigliano M, Lai CG (2010) Probabilistic seismic hazard macrozonation of Tamil Nadu in Southern India. *Bull Seismol Soc Am* 100(3):1320–1341
- Mir R (2020) *Crustal structure and quantified earthquake hazard in the North Western Himalaya*. Dissertation, Academy of Scientific and Innovative Research, New Delhi, India
- Mittal H, Kumar A (2015) Stochastic finite-fault modeling of M_w 5.4 earthquake along Uttarakhand-Nepal border. *Nat Hazards* 75(2):1145–1166
- Mohadjer S, Ehlers TA, Bendick R, Stübner K, Strube T (2016) A quaternary fault database for central Asia. *Nat Hazards Earth Syst Sci* 16:529–542. <https://doi.org/10.5194/nhess-16-529-2016>
- Motazedian D, Atkinson GM (2005) Stochastic finite-fault modeling based on a dynamic corner frequency. *Bull Seismol Soc Am* 95(3):995–1010. <https://doi.org/10.1785/0120030207>
- Okawa I (2005) Strong earthquake motion recordings during the Pakistan, 2005/10/8, Earthquake. Technical report. <https://iisee.kenken.go.jp>
- Panjamani A, Bajaj K, Moustafa SS, Al-Arifi NS (2016) Relationship between intensity and recorded ground-motion and spectral parameters for the Himalayan region. *Bull Seismol Soc Am* 106(4):1672–1689
- Panza GF, Romanelli F, Vaccari F (2001) Seismic wave propagation in laterally heterogeneous elastic media: theory and applications to seismic zonation. *Adv Geophys* 43:1–95
- Parvez IA, Gusev AA, Panza GF, Petukhin AG (2001) Preliminary determination of the interdependence among strong-motion amplitude, earthquake magnitude and hypocentral distance for the Himalayan region. *Geophys J Int* 144(3):577–596
- Parvez IA, Vaccari F, Panza GF (2003) A deterministic seismic hazard map of India and adjacent areas. *Geophys J Int* 155(2):489–508
- Parvez IA, Magrin A, Vaccari F, Ashish, Mir RR et al (2017) Neo-deterministic seismic hazard scenarios for india—a preventive tool for disaster mitigation. *J Seismol*. <https://doi.org/10.1007/s10950-017-9682-0>

- Rodriguez-Marek AD, Bray J, Abrahamson N (2001) An empirical geotechnical seismic site response procedure. *Earthq Spectra* 17(1):65–87
- Rout MM, Das J, Kamal, Das R (2015) Probabilistic seismic hazard assessment of NW and central Himalayas and the adjoining region. *J Earth Syst Sci* 124(3):577–586. <https://doi.org/10.1007/s12040-015-0565-x>
- Sapkota SN, Bollinger L, Klinger Y, Tapponnier P et al (2013) Primary surface ruptures of the great Himalayan earthquakes in 1934 and 1255. *Nat Geosci* 6(1):71–76. <https://doi.org/10.1038/ngeo1669>
- Scordilis EM (2006) Empirical global relations converting MS and mb to moment magnitude. *J Seismol* 10(2):225–236. <https://doi.org/10.1007/s10950-006-9012-4>
- Sun X, Hartzell S, Rezaeian S (2015) Ground-motion simulation for the 23 August 2011, Mineral, Virginia, earthquake using physics-based and stochastic broadband methods. *Bull Seismol Soc Am* 105(5):2641–2661
- Wells DL, Coppersmith KJ (1994) New empirical relationships among magnitude, rupture length, rupture width, rupture area, and surface displacement. *Bull Seismol Soc Am* 84(4):974–1002
- Wiemer S (2001) A software package to analyse seismicity: ZMAP. *Seism Res Lett* 72(2):373–382. <https://doi.org/10.1785/gssrl.72.3.373>
- Yeats RS, Thakur VC (1998) Reassessment of earthquake hazard based on fault- bend fold model of the Himalayan plate-boundary fault. *Curr Sci* 74(3):230–233
- Zuccolo E, Vaccari F, Peresan A et al (2011) Neo-deterministic and probabilistic seismic hazard assessments: a comparison over the Italian territory. *Pure Appl Geophys* 168:69–83. <https://doi.org/10.1007/s00024-010-0151-8>

Publisher's Note Springer Nature remains neutral with regard to jurisdictional claims in published maps and institutional affiliations.

Affiliations

Ramees R. Mir^{1,2}  · Imtiaz A. Parvez^{1,2}

✉ Ramees R. Mir
ramizmir752@gmail.com

¹ CSIR-Fourth Paradigm Institute, Wind Tunnel Road, Bangalore 560037, India

² Academy of Scientific and Innovative Research (AcSIR), Ghaziabad 201002, India